Precision spectroscopy of Li I and II

J. J. Clarke and W. A. van Wijngaarden
Physics Department, Petrie Bldg., York University, 4700 Keele St.
Toronto, Ontario, M3J 1P3, Canada

Abstract

Recent advances in theory have renewed interest in precision measurements for 2 and 3 electron systems. This paper reviews measurements of the Li^+ $1s2s$ $^3S \rightarrow 1s2p$ ^3P transition and the neutral lithium D lines. It also discusses a new technique where an electro-optically modulated laser beam is frequency scanned across the resonance of either an ion or neutral beam. The linearity of the laser scan is corrected by passing part of the laser beam through an etalon. The free spectral range of the etalon is separately calibrated for each scan using the electro-optic modulation frequency permitting important consistency checks. The results for the isotope shift, fine and hyperfine splittings are more accurate than previous experiments and resolve significant discrepancies in the literature.

1. Introduction

Two electron systems such as helium and Li^+ are the simplest atoms containing the electron-electron interaction. The helium spectrum has been studied extensively in

Correspondence/Reprint request: Dr. W. A. van Wijngaarden, Physics Department, Petrie Bldg., York University, 4700 Keele St. Toronto, Ontario, M3J 1P3, Canada . E-mail: wavw@yorku.ca

numerous experiments [1–5]. Analytical solutions to the Schrödinger equation, however, have not been found. Recent theoretical advances have been made using a variational technique with a Hylleraas double basis set [6, 7]. Comparison of experiment with this theory provides a stringent test of our understanding of two and three electron systems [8–14]. In particular, information is obtained about quantum electrodynamic (QED) contributions that scale to lowest order as $Z^4 \alpha^3$ times the Rydberg energy, where Z is the nuclear charge and $\alpha = e^2 / \hbar c$ is the fine structure constant. Here, e is the electron charge, c is the speed of light and $\hbar = h/2\pi$ where h is Planck's constant. Hence, QED effects are more prominent in lithium than in either helium or hydrogen [1]. Accurate measurement of Li^+ state energies is also needed to test special relativity [15] and the theoretical models are also sensitive to the nuclear size. Indeed, high precision measurements of isotope shifts can yield information that is substantially more accurate than that obtained in nuclear scattering experiments [16].

Lithium is a particularly attractive system for an experimentalist. It is an alkali metal that naturally occurs in two isotopes (92.58% ^7Li, 7.42% ^6Li). The relatively low melting point of 180.5 C facilitates the production of an atomic beam. Lithium has a weakly bound valence electron with an ionization energy of only 5.392 eV. Therefore, an ion beam is readily generated by colliding electrons with a beam of neutral lithium atoms. A transition exists from the metastable Li^+ $1s2s$ $^3S_1$ state at 548.5 nm where narrow linewidth dye laser technology conveniently operates. Similarly, the Li D lines are excited by 670 nm light that can be generated by either diode or dye lasers.

Two experimental groups have published sharply disagreeing results for Li^+ transition frequencies as well as fine structure (FS) intervals [16–20]. In the case of neutral lithium, results obtained using a laser to excite an atomic beam and thereby measure the $^{6,7}Li$ isotope shifts as well as the fine and hyperfine structure (HFS) splittings of the Li D lines have been found to be in error due to problems calibrating Fabry Perot interferometers [21–25]. Recently, an experimental technique was devised whereby an ion or neutral atomic beam was excited by a frequency modulated laser beam [26–31]. This technique has definitively resolved the experimental discrepancies in Li^+ and yielded results that have challenged theory in the case of neutral Li.

This paper is organized as follows. First, the variational theory as applied to two electron atomic systems is discussed. Section 3 reviews previous work that studied the Li^+ $1s2s$ $^3S \rightarrow 1s2p$ ^3P transition. Our experiment is next described and the results for the fine and hyperfine structure splittings are compared to previous data. Section 4 presents an overview of the various methods used to study the Li D lines. It then presents recent measurements of the $^{6,7}Li$ D1 isotope shift as well as the hyperfine and fine structure of the $2S_{1/2}$ and $2P_{1/2,3/2}$ states. Conclusions are given in Section 5.

2. Theoretical background

The Schrödinger equation for a two electron atom is [32]:

$$\left[\frac{1}{2M} \vec{P}_N^2 + \frac{1}{2m_e} \sum_{i=1}^{2} \vec{P}_i^2 + V(\vec{R}_N, \vec{R}_1, \vec{R}_2) \right] \Psi = E\Psi \tag{1}$$

where M is the mass of the nucleus, m_e is the electron mass, Ψ is the wavefunction, and E is the corresponding eigenenergy. $\vec{R}_N$, $\vec{R}_1$ and $\vec{R}_2$ are the position vectors of the

nucleus and the two electrons respectively. The nuclear momentum operator is $\vec{P_N} = (\hbar/i)\nabla_N$ while the electron momentum operator is $\vec{P_i} = (\hbar/i)\nabla_i$. The Coulomb potential is

$$V(\vec{R_N}, \vec{R_1}, \vec{R_2}) = -\frac{Ze^2}{|\vec{R_N} - \vec{R_1}|} - \frac{Ze^2}{|\vec{R_N} - \vec{R_2}|} + \frac{e^2}{|\vec{R_1} - \vec{R_2}|} \tag{2}$$

This equation can be simplified by the change of variables

$$\vec{r_i} = \vec{R_i} - \vec{R_N} \tag{3}$$

$$\vec{X} = \frac{M\vec{R_N} + m_e\vec{R_1} + m_e\vec{R_2}}{M + 2m_e} \tag{4}$$

$$\mu = \frac{m_e M}{m_e + M} \tag{5}$$

where $\vec{X}$ is the center of mass position and μ is the reduced mass of the electron.

It is convenient to express variables as dimensionless quantities. The values of μ/M are $9.121677(1) \times 10^{-5}$ for ^{6}Li$^+$ and $7.820203(1) \times 10^{-5}$ for ^{7}Li$^+$ [6, 33]. In particular, Eqn. 1 simplifies with the following change of scale

$$\vec{\rho_i} = \frac{\vec{r_i}}{a_\mu} \tag{6}$$

$$\epsilon = \frac{E}{e^2/a_\mu} \tag{7}$$

where $a_\mu = (m_e/\mu)a_0$. $a_0 = \alpha/(4\pi R_\infty)$ is the Bohr radius, and $R_\infty = m_e c \alpha^2/2h$ is the Rydberg constant for a nucleus of infinite mass. Using Eqns. 3 – 7 in Eqn. 1 yields

$$\left[-\frac{1}{2}\sum_{i=1}^{2}\nabla^2_{\rho_i} + H_{mp} + V(\vec{\rho_1}, \vec{\rho_2}) \right]\Psi = \epsilon\Psi \tag{8}$$

where V is the potential energy in units of e^2/a_μ

$$V(\vec{\rho_1}, \vec{\rho_2}) = -\frac{Z}{\rho_1} - \frac{Z}{\rho_2} + \frac{1}{|\vec{\rho_1} - \vec{\rho_2}|} \tag{9}$$

Eqn. 8 has a form similar to the Schrödinger equation with an additional term H_{mp} called the mass polarization given by

$$H_{mp} = -\frac{\mu}{M} \nabla_{\rho_1} \cdot \nabla_{\rho_2} \qquad (10)$$

Eqn. 8 must be solved numerically using techniques such as the Rayleigh-Ritz variational principle [32] as an analytic solution has yet to be discovered. In the Hylleraas approach to the variational technique a trial wavefunction is constructed as follows

$$\Psi_{tr} = \sum_{l_1=0}^{L/2} \sum_{p=1}^{N} C_{pl_1} \chi_p r_1^{l_1} r_2^{l_2} \gamma_{l_1 l_2 L}(\hat{r}_1, \hat{r}_2) \pm exchange \qquad (11)$$

where C_{pl_1} are the variational parameters. $\gamma_{l_1 l_2 L}(\hat{r}_1, \hat{r}_2)$ given by

$$\gamma_{l_1 l_2 L}(\hat{r}_1, \hat{r}_2) = \sum_{m_1, m_2} Y_{l_1 m_1}(\hat{r}_1) Y_{l_2 m_2}(\hat{r}_2) \langle l_1 l_2 m_1 m_2 | LM \rangle \qquad (12)$$

$\hat{r}_1$ and $\hat{r}_2$ is a shorthand notation for the angles θ_1, ϕ_1 and θ_2, ϕ_2 corresponding to the vectors $\vec{r}_1$ and $\vec{r}_2$ expressed in spherical coordinates. Here, m_1 and m_2 are the azimuthal components of the orbital angular momenta l_1 and l_2 of the two electrons. M is the azimuthal component of L, the total electronic orbital angular momentum. Y_{lm} are spherical harmonic functions and $\langle l_1 l_2 m_1 m_2 | LM \rangle$ is the Clebsch-Gordan coefficient. The components of the basis set $\{\chi_p\}$ are given by

$$\chi_p(\alpha, \beta) = r_1^i r_2^j r_{12}^k e^{-\alpha r_1 - \beta r_2} \qquad (13)$$

whre $r_{12} = |\vec{r}_1 - \vec{r}_2|$. The distance scale is set by α and β. p is an index labelling triplets of nonmegative integers $\{i, j, k\}$.

The trial wavefunction given by Eqn. 11 has been chosen to resemble the product of hydrogenic wavefunctions. The wavefunction approaches zero in the limit as $r_1, r_2 \rightarrow \infty$ since bound electrons are located near the nucleus. Eqn. 11 does not explicitly contain the spin part of the wavefunction. The Pauli exclusion principle is accounted for by the exchange term where the plus sign applies for singlet states and the negative sign for triplet states.

The technique has been extended by forming a so called double Hylleraas basis set [6]

$$\Psi_{tr} = \sum_{l_1=0}^{L/2} \sum_{p} [C_{pl_1}^1 \chi_p(\alpha_1, \beta_1) + C_{pl_1}^2 \chi_p(\alpha_2, \beta_2)] r_1^{l_1} r_2^{l_2} \gamma_{l_1 l_2 L}(\hat{r}_1, \hat{r}_2) \pm exchange \qquad (14)$$

where $C_{pl_1}^1$ and $C_{pl_2}^2$ are the variational parameters, $\gamma_{l_1 l_2 L}(\hat{r}_1, \hat{r}_2)$ and χ_p are as given by Eqns. 12 and 13 respectively. This basis set contains two sets of terms that represent different distance scales α_1, β_1 and α_2, β_2 for each p.

The precision obtained using the Hylleraas technique is limited by the number of terms used to construct the wavefunction. This increases rapidly as the maximum values of i, j, k increase and the computer time becomes very large. In practice, wavefunctions of up to 2000 terms have been used [6].

The variational calculations of G.W.F. Drake et al are done by first determining the wavefunction corresponding to the Hamiltonian given in Eqn. 8 neglecting the mass polarization term. The resulting so called nonrelativistic wavefunctions correspond to eigenenergies E_o that for the case of helium have been found to one part in 10^{16} [6]. Perturbation theory is then used to evaluate higher order terms allowing the energy of a state to be expressed as follows.

$$E = E_o + \frac{\mu}{M}E_{01} + \left(\frac{\mu}{M}\right)^2 E_{02} + \alpha^2 E_{20} + \alpha^2 \frac{\mu}{M}E_{21} + \alpha^3 E_A$$

$$+ E_{nuc} + E_{hyp} + E_{L1} + E_{L2} \tag{15}$$

Here, the E_{01} and E_{02} terms result from considering the effect of the mass polarization operator given in Eqn. 10 using first and second order perturbation theory. The next term proportional to E_{20} arises from the Breit interaction [1] that encompasses the fine structure. E_{21} is a higher order correction arising from both the Breit interaction and the mass polarization Hamiltonian. The E_A term results from the anomalous magnetic moment of the electron. E_{nuc} is the perturbation to the Coulomb potential inside a nucleus having a root mean square charge radius R. It equals the expectation value of the operator:

$$H_{nuc} = \frac{2\pi Z}{3}(R/a_0)^2 \left[\delta(\vec{r_1}) + \delta(\vec{r_2})\right] \tag{16}$$

This term only contributes significantly for S states because of the three dimensional delta function $\delta(\vec{r})$. E_{hyp} represents the hyperfine splitting that is dominated by the magnetic dipole and electric quadrupole moments of the nucleus. QED corrections give rise to the last two terms in Eqn. 15 [34, 35]. E_{L1} is the electron-nucleus Lamb shift.

$$E_{L1} = \frac{Z^4 \alpha^3}{\pi n^3}\Big[A_0 + A_1 \ln(Z\alpha) + Z\alpha A_2$$
$$+ (Z\alpha)^2[A_3 \ln^2(Z\alpha) + A_4 \ln(Z\alpha) + A_5] + O(Z\alpha)^3\Big] \tag{17}$$

A_{0-4} are coefficients calculated from various Feynman diagrams and A_0 is dominated by the so called Bethe logarithm term, E_{L2} is the Araki-Sucher electron-electron QED correction. It is given by an expression similar to Eqn. 17 but with $Z = 1$.

$$E_{L2} = \alpha^3 \Big[B_0 + B_1 \ln \alpha + B_2 \alpha + O(\alpha^2)\Big] \tag{18}$$

The calculations of state energies incorporating the Hylleraas double basis set in the Variational Principle are elaborate. Therefore, comparison to precise measurements of fine and hyperfine structure splittings as wells as isotope shifts a) test the accuracy of the numerical computations and b) confirm whether all relevant physics has been included in the perturbative expansion of the state energy as given in Eqn. 15.

3. Spectroscopy of Li^+ 1s2s $^3S \rightarrow$ 1s2p ^3P transition

3.1 Review of previous experiments

The low-lying energy states of Li^+ are illustrated in Fig. 1. We are interested in the transition from the 1s2s $^3S_1$ state. This state has a long lifetime, measured to be 59 ± 13 s [36], since an electric dipole transition to the ground state violates various angular momentum selection rules. The 1s2s $^3S_1 \rightarrow$ 1s2p ^3P transition occurs at 548 nm. The 1s2p ^3P state has a lifetime of 43 ns [37]. The branching ratio of the 1s2p ^3P state to the 1s2s $^3S_1$ state is several orders of magnitude larger than for other decay channels to $^1S_0$ states [38]. Hence, a given Li^+ can be cycled many times between the 1s2s ^3S and 1s2p ^3P states before it decays to the Li^+ ground state.

The fine and hyperfine structure splittings of the 1s2s ^3S and 1s2p ^3P states are shown in Figs. 2 and 3 for $^6Li^+$ and $^7Li^+$ respectively along with the possible laser excitations. F denotes the hyperfine level and is the sum of the nuclear spin and total electronic angular momentum J. The 1s2s $^3S \rightarrow$ 1s2p ^3P transition has been studied by various techniques. This paper reviews experiments yielding data with uncertainties not more than an order of magnitude greater than our work.
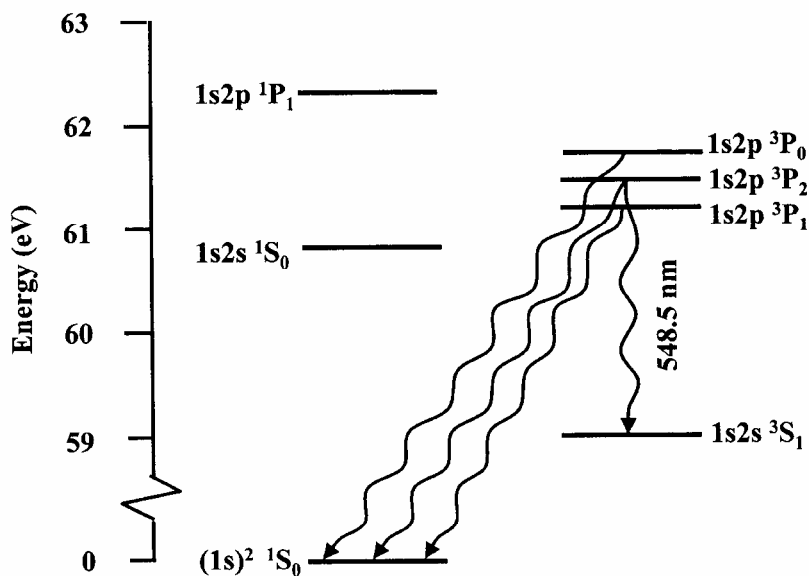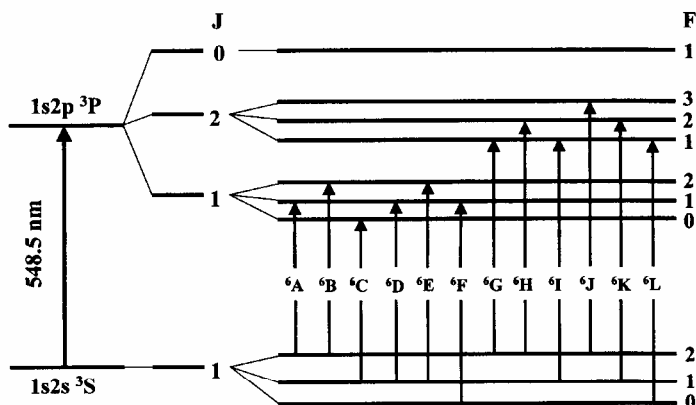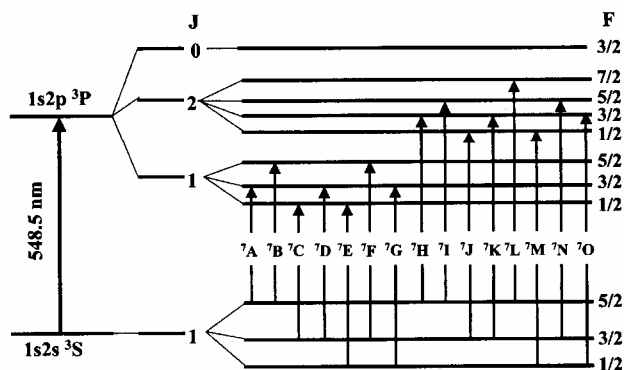

Figure 1. Low-Lying Li^+ Energy States. The vertical energy scale is not drawn to scale.

Figure 2. Hyperfine Levels Involved in ^{6}Li$^+$ 1s2s ^{3}S → 1s2p ^{3}P Transition. The vertical energy axis is not drawn to scale.

Figure 3. Hyperfine Levels Involved in ^{7}Li$^+$ 1s2s ^{3}S → 1s2p ^{3}P Transition. The vertical energy axis is not drawn to scale.

3.1.1 Laser ion beam spectroscopy

Laser ion beam spectroscopy (LIB), illustrated in Fig. 4, was used by the group of Bayer [39, 40] to measure the fine and hyperfine structure splittings as well as the isotope shift of the ^{6,7}Li$^+$ 1s2s ^{3}S → 1s2p ^{3}P transition. An oven was heated to 500 - 600 C to generate a beam of neutral lithium atoms. Ions were produced by bombarding the atomic beam with a 40 mA electron beam. The Li ions were accelerated to an energy of 200 - 300 eV and collimated using an electrostatic lens. The Li$^+$ current was measured to be 1 μA. The fraction of Li$^+$ emerging in the metastable 1s2s ^{3}S state was estimated to be one part in 10^3.

A dye laser beam intersected the Li$^+$ beam perpendicularly to minimize the first order Doppler shift. The laser linewidth was 1 MHz and the frequency could be scanned over 60 GHz without modehops. Fluorescence, produced by the radiative decay of the 1s2p ^{3}P state, was detected by a cooled photomultiplier (PMT) as the laser frequency
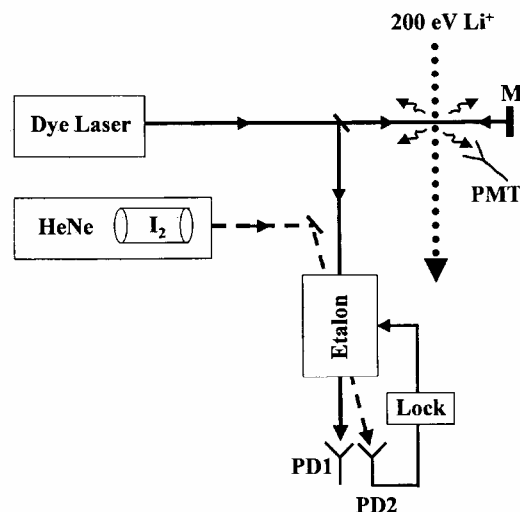
Figure 4. Laser Excitation of Ion Beam Apparatus

was scanned across the resonance. Lamb dips in the fluorescent signals were generated by retro-reflecting the laser beam back through the ion beam. The FWHM (fullwidth at half maximum) of the Lamb dips was 100 MHz. This significantly exceeded the 3.7 MHz natural linewidth of the transition, due to power broadening and the finite transit time of the ions passing through the laser beam. The dye laser frequency scan was calibrated using a photodiode (PD1) that recorded the transmission of part of the dye laser beam through an etalon. The etalon length was locked using an iodine stabilized HeNe laser.

Hyperfine splittings of the $^{6,7}Li^+$ 1s2s ^3S and 1s2p ^3P states and fine structure splittings of the 1s2p ^3P state were determined with a 3σ uncertainty of between 4 and 25 MHz. The major factor contributing to this uncertainty was the determination of the center of small Lamb dip signals that for some transitions were obscured by overlapping neighboring peaks.

3.1.2 Doppler tuning

Doppler tuning (DT) a laser into resonance with an ion beam is illustrated in Fig. 5. This technique was used by Fan et al [41, 42] to measure the $^{6,7}Li^+$ 1s2s $^3S_1$ and 1s2p $^3P_{1,2}$ hyperfine splittings. A Li^+ beam was generated using a modified ion-implantation machine (Extrion-50KV) and a mass filter. The authors estimate that approximately 10^{-6} to 10^{-7} of the 2 μA Li^+ beam was in the 1s2s ^3S state. The dye laser frequency remained constant throughout the experiment. Fluorescence was recorded by a cooled photomultiplier (PMT) while the ion beam velocity was scanned causing the resonance frequency to be Doppler tuned. The latter was accomplished by applying a voltage ramp to a metal box containing the segment of the ion beam monitored by the PMT.

Fluorescence emitted in the direction perpendicular to the ion velocity was detected. The lineshape was observed to be asymmetric and strongly affected by fluctuation of ion source voltages. These instabilities limited the determination of the total accelerating voltage to an uncertainty of 0.05% and broadened the FWHM linewidth of the fluorescent peak to 450
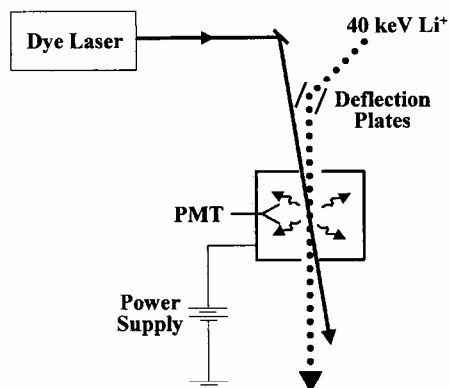
Figure 5. Doppler Tuning Apparatus

MHz. The ^{6,7}Li$^+$ 1s2s ^{3}S and 1s2p ^{3}P hyperfine splittings were determined with a 2σ uncertainty of between 6 and 24 MHz.

3.1.3 Laser microwave

The laser microwave (LM) technique, illustrated in Fig. 6 was used by the zu Putlitz group [37] to measure the hyperfine splittings of the ^{6,7}Li$^+$ 1s2s ^{3}S$_1$ state. An ion beam was generated as described in Section 3.1.1. A dye laser beam that was modulated at 2 kHz by a chopper, perpendicularly intersected the ion beam. The laser frequency was tuned to the 1s2s ^{3}S$_1$(F) $\rightarrow$ 1s2p ^{3}P$_{1,2}$(F$'$)transition. A cooled photomultiplier (PMT1) monitored fluorescence produced from the radiative decay of the 1s2p ^{3}P state.
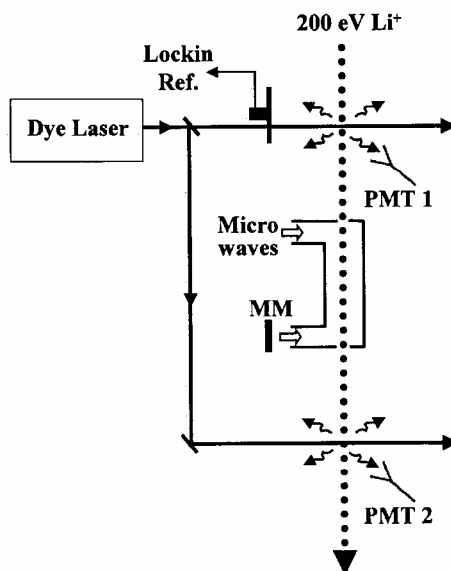

Figure 6. Laser Microwave Apparatus

The laser excitation depopulated one of the 1s2s $^3S_1$ hyperfine levels by optical pumping. The ion beam then passed through a waveguide containing a microwave field. The microwaves repopulated the hyperfine level depleted by the initial laser excitation. The ions were also laser excited after the microwave cavity and fluorescence was monitored using a second cooled photomultiplier (PMT2). The signals had a 0.5 - 1.3 MHz FWHM width that was dominated by time-of-flight broadening. The $^{6,7}Li^+$ 1s2s $^3S_1$ hyperfine splittings were determined with a 3σ uncertainty of 0.04 - 0.05 MHz. The 1s2p ^3P hyperfine splittings were also found using this technique. However, the uncertainty (0.5 - 2 MHz) was larger because the natural linewidth of the 1s2p ^3P state is sub-stantially greater than that of the metastable 1s2s ^3S state.

3.1.4 Laser heterodyne

The laser heterodyne (LH) technique is illustrated in Fig. 7. It was used by Rong et al [18] to measure the fine structure splittings of the $^7Li^+$ 1s2p ^3P state. A Li^+ beam was generated using the ion source described in Section 3.1.1. A ring dye laser beam (Dye Laser 1) intersected the ion beam. The laser linewidth was 1 MHz and the frequency could be scanned up to 30 GHz without modehops. A mirror (M) retro-reflected the laser beam back through the ion beam. Fluorescence produced by the radiative decay of the 1s2p ^3P state was monitored by a cooled photomultiplier (PMT) as the laser frequency was scanned across the 1s2s $^3S \rightarrow$ 1s2p ^3P resonance. The fluorescent peaks were observed to consist of a 200 MHz FWHM Lamb dip superimposed on a 2 GHz FWHM Doppler broadened lineshape. The Doppler background was removed by subtracting data collected with the retro-reflected laser beam blocked. A second ring dye laser (Dye Laser 2) with a 1 MHz linewidth was locked to an iodine transition using saturated absorption spectroscopy.
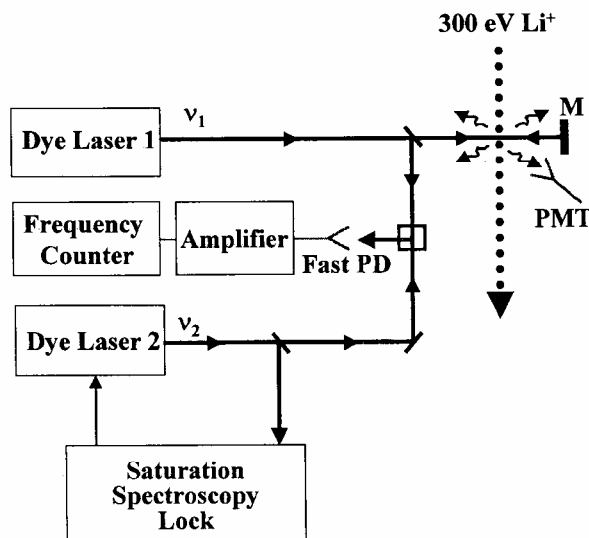

Figure 7. Laser Heterodyne Apparatus

The frequency difference between Dye Lasers 1 and 2 was found by focusing part of each laser beam onto a fast avalanche photodiode (Fast PD). The output of the diode was a beat signal at the frequency difference $v_2 - v_1$. The response time of the diode limited the maximum detectable frequency difference to 12.5 GHz. Beat signals of up to 4 GHz were measured directly by a frequency counter while signals between 4 and 12.5 GHz were first amplified. The frequency counter was calibrated using a Cs frequency standard and found to be accurate to one part in 3×10^6. Frequency intervals of up to 150 GHz were found by measuring multiple smaller intervals using intermediate iodine lines to lock Dye Lasers 1 and 2.

This technique was tested by measuring the $^7Li^+$ 1s2s $^3S_1$ (F = 5/2 → F = 3/2) interval. The result of 19,817.1 ± 2.6 MHz was in good agreement with 19,817.673 ± 0.040 MHz obtained using the laser microwave technique. The $^7Li^+$ 1s2p ^3P fine structure intervals were measured with a 3σ uncertainty of 2 MHz.

3.1.5 Absolute frequency measurements

Absolute transition frequencies (AFM) were measured by Riis et al [16, 17] for the $^{6,7}Li^+$ 1s2s $^3S_1$ → 1s2p $^3P_{0,1,2}$ transitions. A discharge ion source generated a beam of Li^+ at an energy of 100 keV. A 90° bending magnet selected the isotope of interest and permitted the ion beam to overlap two counter-propagating dye laser beams. The laser beams were generated by two ring dye lasers that were each frequency locked to an iodine transition. One dye laser co-propagated with the ions and was Doppler tuned into resonance with one of the $^{6,7}Li^+$ 1s2s $^3S_1(F)$ → 1s2p $^3P_J(F')$ transitions. A photomultiplier recorded fluorescence from the radiative decay of the 1s2p ^3P state as the frequency of the second dye laser was scanned across the resonance using an acousto-optic modulator (AOM) as shown in Fig. 8. The observed fluorescence peak was a 25 MHz FWHM Lamb dip superimposed on a 100 MHz FWHM Doppler broadened lineshape. The Doppler background was removed from the signal to isolate the Lamb dip by subtracting data taken with the first dye laser beam blocked.

The absolute frequencies of the dye lasers, v_{Dye} were estimated with an uncertainty of 30 MHz using a wavemeter. This relatively crude measurement was confirmed using the iodine atlas [43]. A more precise determination of the laser frequency was made using an evacuated 1 m Fabry Perot etalon. A photodiode (PD1) monitored the transmission of part of the dye laser beam through the etalon. This signal was used to lock the etalon length, by applying a voltage to a piezoelectric crystal on which an etalon mirror was mounted. A second photodiode (PD2) monitored the transmission of a HeNe laser beam through the etalon. The HeNe laser frequency, v_{HeNe}, was locked to maximize this transmission signal. The dye and HeNe laser frequencies were integer multiples M and N respectively of the etalon free spectral range. These integers were determined using the initial coarse wavelength measurement and the known etalon length. The ratio, R, of the dye and HeNe laser frequencies, was given by

$$R = \frac{v_{Dye}}{v_{HeNe}} = \frac{M - f}{N} \tag{19}$$

where f is the fringe fraction due to the wavelength dependence of the mirror coatings. It was found by comparing data recorded using the same mirrors but with a different etalon
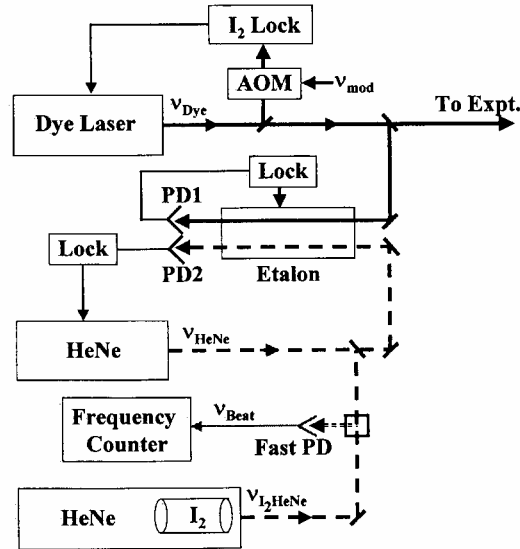
Figure 8. Absolute Frequency Measurement Apparatus

length. ν_{HeNe} was determined by focusing parts of the HeNe laser beam and a separate I_2 stabilized HeNe laser beam onto a fast photodiode and measuring the beat signal.

$$\nu_{Beat} = \nu_{I_2HeNe} - \nu_{HeNe} \tag{20}$$

The absolute frequency of the dye laser was then found using Eqn. 19.

The fine structure splittings of the 1s2p ^{3}P states were determined with an uncertainty of about 0.5 MHz by taking differences of the measured absolute transition frequencies. The precision was limited by the linewidth of the Lamb dip and the uncertainty of the iodine transition frequency used to lock the HeNe laser.

3.2 Laser excitation of ion beam using an electro-optic modulator

The technique whereby an ion beam is excited by an electro-optically modulated laser beam (LIBEO) is illustrated in Fig. 9. The Li$^+$ beam was generated using an ion source that is described in detail elsewhere [44]. A sample of either natural or isotopically purified (99% ^{6}Li) lithium was first outgassed in a separate vacuum chamber. A neutral lithium atomic beam was produced by an oven heated to 650 C and collimated by a 3.8 mm diameter aperture. Ions were produced by intersecting the atomic beam with a 80 mA beam of 500 eV electrons. The ions were extracted and accelerated using a 6 kV power supply (Fluke 408b) that had a ripple of less than 1 mV RMS. The high voltage was monitored using a 1/5000 voltage divider (Julie Research Labs KV-50) having an accuracy of 0.02% and a precision voltmeter (Hewlett Packard 34401A). A voltage stability of better than 5 parts in 10^6 was observed throughout the experiment. Approximately 1% of the Li$^+$ emerged from the source in the 1s2s ^{3}S$_1$ state [44]. The ions propagated in the $\hat{z}$ direction and were focused by an Einzel lens into a
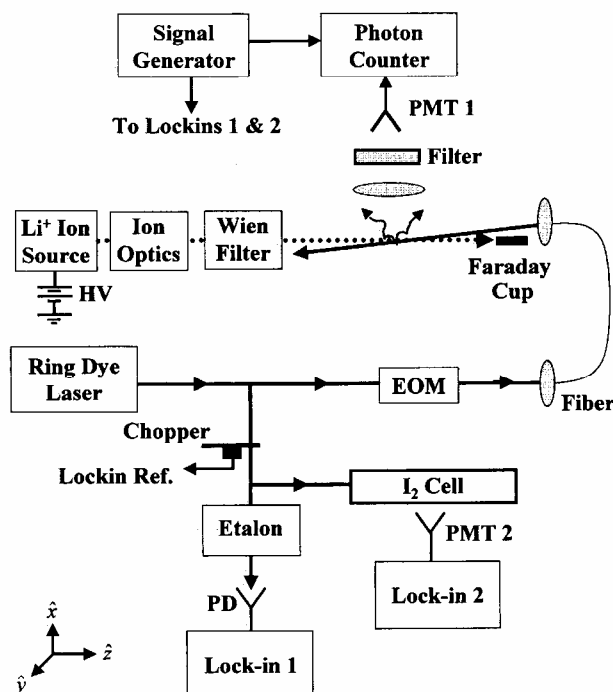
Figure 9. Laser Excitation of Ion Beam using an Electro-optic Modulator Apparatus

Wien velocity filter. A Faraday cup located 1.3 m from the Wien filter measured a Li^+ current of 250 nA. The ion beam propagated in a vacuum chamber maintained at a pressure of 1×10^{-7} torr using two diffusion pumps and liquid nitrogen traps.

Laser radiation was supplied by a CW ring dye laser (Coherent 669) that generated in excess of 600 mW at 548 nm using pyromethene 556 laser dye. The dye laser had a linewidth of less than 1 MHz and could be tuned 30 GHz without modehops. The frequency was monitored by passing part of the laser beam through an iodine cell and observing the fluorescence with a photomultiplier (PMT2). The signal was analyzed by a lock-in amplifier (Lock-in 2).

The dye laser beam passed through one of two electro-optic modulators (EOM - v-focus 4851) operating at either 6.8 or 9.2 GHz. The modulation frequency was specified to better than one part in 10^7 using a frequency synthesizer (Agilent E8241A). The modulation frequency was amplified (Quinstar QPN-08403534) to a power of up to 3 W. The laser beam emerging from the EOM was focused into a single mode polarization maintaining fiber (Thorlabs FS-PM-2021) with a coupling efficiency of 70%. The fiber ensured the 15 mrad angle of intersection of the laser and ion beams remained constant. The laser beam was retroreflected by a mirror not shown in Fig. 9. Data was taken using calibrated neutral density filters to vary the laser power from 1 to 10 mW.

Fluorescence produced by the radiative decay of the $1s2p$ ^3P state was detected using a f/1.5 optical system. Laser scatter was reduced using an interference filter (Omega

550BP10) having a bandwidth of 10 nm centered at 550 nm as well as a spatial filter. A liquid nitrogen cooled photomultiplier (PMT1 - Hamamatsu R943-02) detected the fluorescence. The PMT1 signal was first processed by a preamplifier (Stanford Research Systems SR445) and then sent to a photon counter (SR430) that recorded data at a rate of 40 Hz. A datafile containing 25,000 data points was recorded for each 30 GHz scan.

Fig. 10 shows a $^6Li^+$ $1s2s$ $^3S_1 \rightarrow 1s2p$ $^3P_2$ spectrum recorded with a) an unmodulated laser beam and b) 1.7 W of $\nu_{MOD} = 9.200000$ GHz microwave power applied to the electro-optic modulator. The ion beam was accelerated by a 5 kV potential. In Fig. 10b, the various transitions were excited multiple times by the frequency sidebands of the laser beam. For example, the interval between peaks ^6J and $^6J^+$ equals ν_{MOD}. The background was dominated by scattered laser light (90%) and ion collisions with residual gas atoms (10%). Fig. 11 shows the excitation of various peaks in $^7Li^+$. The labels of the peaks shown in Figs. 10 and 11 correspond to the transitions indicated in Figs. 2 and 3. The n+/n- superscripts indicate that the transition was excited the laser sideband shifted by $\pm n\nu_{MOD}$ from the unshifted dye laser frequency.

Fig. 12 shows the $^6Li^+$ $1s2s$ $^3S_1 \rightarrow 1s2p$ $^3P_2$ spectrum for a) co- and b) counter-propagating ion and laser beams. In both cases a 4981 V potential accelerated the ions. The velocity distribution of the ions determined the asymmetric lineshape, which was inverted in Fig. 12a relative to Fig. 12b. Only one day of data was taken for counter-propagating beams since partially overlapping peaks such as ^6K and ^6L were more clearly resolved using co-propagating ion and laser beams.
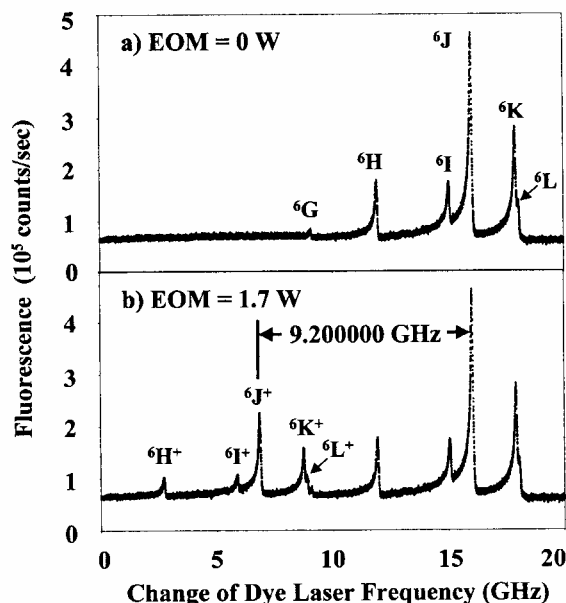
Figure 10. Sample $^6Li^+$ $1s2s$ $^3S_1 \rightarrow 1s2p$ $^3P_2$ Spectrum. This was obtained using a 9.200000 GHz electro-optical modulator with a) 0 W and b) 1.7 W of modulation power supplied to the EOM.
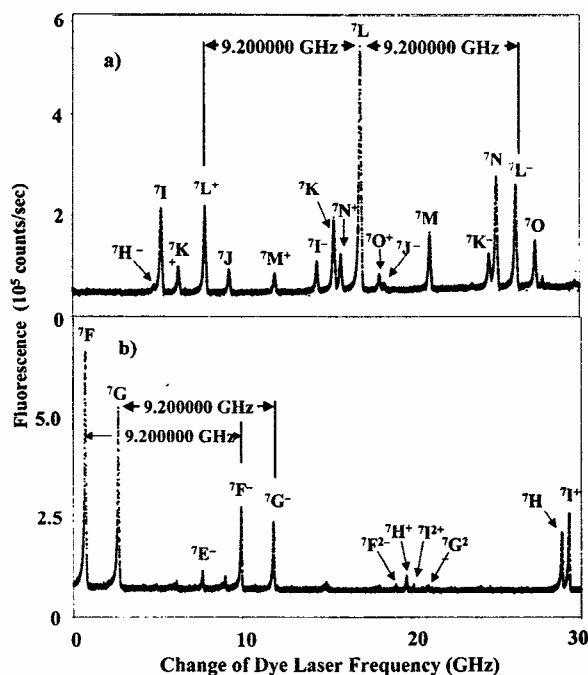
Figure 11. Sample $^7Li^+$ 1s2s $^3S_1 \to$ 1s2p ^3P Spectrum. This was obtained using a 9.200000 GHz electro-optical modulator for the excitation of the a) 1s2p $^3P_2$ state b) 1s2p $^3P_{1,2}$ states. Scans such as in b) were used to determine the 1s2p ^3P (J = 1 $\to$ J = 2) fine structure interval.
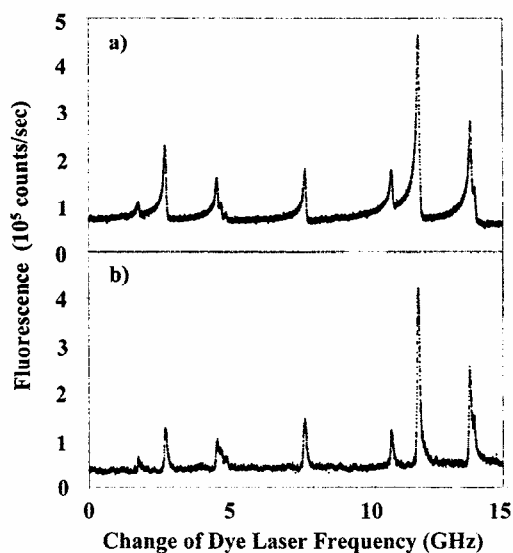
Figure 12. Sample $^6Li^+$ 1s2s $^3S_1 \to$ 1s2p $^3P_2$ Spectrum. This was obtained using a 9.200000 GHz electro-optical modulator for a) co- and b) counter-propagating ion and laser beams.

The first step in the data analysis was to determine the time intervals between the various peaks in each spectrum. The highly asymmetric lineshape is a complex function of the conditions inside the ion source and difficult to model. Instead, the time interval separating two fluorescent peaks was determined directly by scaling the intensity of one peak and translating its temporal position in the scan to optimize its overlap with the second peak. The background was also an adjustable parameter, but had little impact since it was nearly constant throughout the laser scan. A computer program performed a least squares fit such as shown in Fig. 13, where the black (red) points correspond to the $^6J^+$ (scaled ^6J) peaks of Fig. 10.

The above procedure was also used to study partially resolved Li$^+$ peaks. For example, in Fig. 13b the black points correspond to the ^6K and ^6L peaks in Fig. 10. The red points correspond to the ^6J peak in Fig. 10 that was shifted and scaled twice to optimize the overlap with the ^6K and ^6L peaks. This method of determining time intervals between peaks worked well since the highly asymmetric lineshape of the data was observed to remain unchanged throughout a laser scan and even during the several hours required for an entire data acquisition session.

The nonlinearity of the laser frequency scan was investigated by recording the transmission of part of the laser beam through an etalon. An example is shown in Fig. 14, which shows the Li$^+$ spectrum from Fig. 10 along with the etalon transmission signal. The free spectral range of the etalon was nearly 300 MHz. The lock-in amplifier data analysis feature fitted a Gaussian function to each etalon transmission maximum, to determine the etalon peak center.
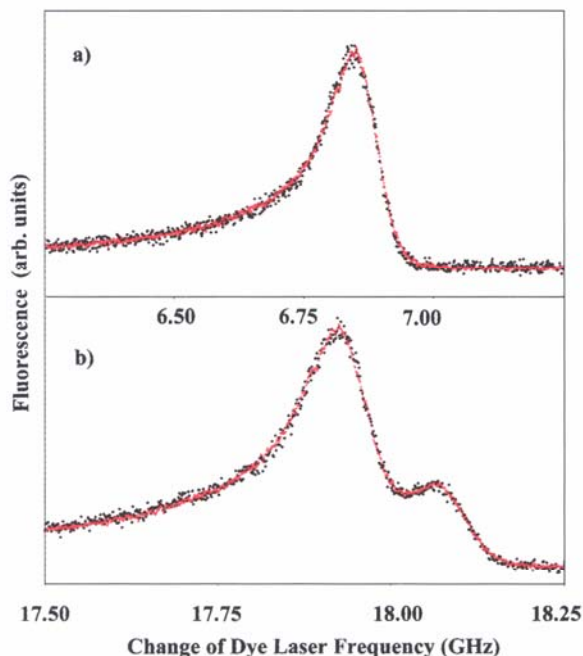

Figure 13. Determination of Frequency Intervals for a) Single and b) Overlapping Peaks.

The laser frequency scan nonlinearity was studied as follows. Ten identical scans like Fig. 14 were taken. The etalon peaks were labelled consecutively starting at 1 for the first transmission maximum in the scan. The average time interval separating each pair of neighboring etalon peaks was plotted versus the etalon peak number as shown in Fig. 15. The time difference corresponding to neighboring free spectral range intervals was less than 0.1% for the first third of the scan and much less for the remainder of the scan. This nonlinearity could result in an error as much as 5 MHz when measuring a 5 GHz interval, if not accounted for. This effect was minimized by measuring the interval between each Li^+ peak and the nearest etalon transmission peak. The maximum error in determining a peak position due to scanning nonlinearity is therefore 0.1% times half of the etalon's free spectral range or 0.15 MHz. For an interval separating two peaks, the two position errors were added in quadrature yielding 0.21 MHz.
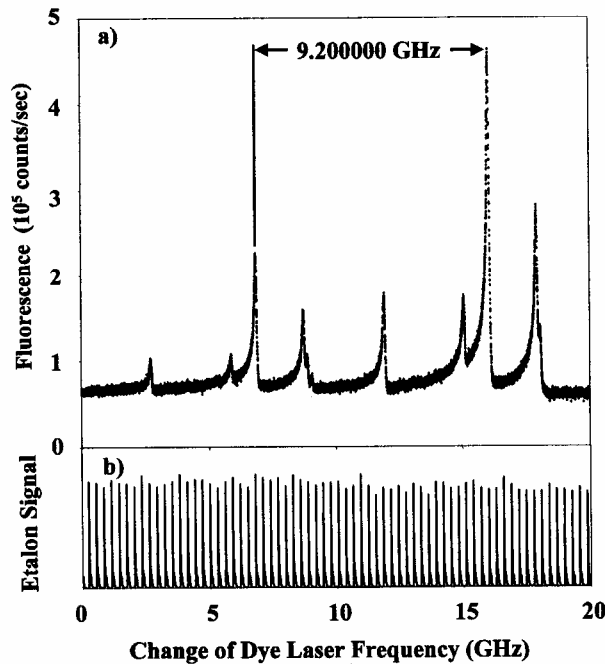
Figure 14. Typical Data. a) shows fluorescence produced when the laser frequency was scanned across the $^6Li^+$ 1s2s $^3S_1$ → 1s2p $^3P_2$ resonance. b) displays the transmission of part of the laser beam through an etalon.

The measured intervals also had to be corrected for the different Doppler shifts of the various transitions. For example, consider the hyperfine interval separating levels 2 and 1 given by $(\nu_2 - \nu_1)_o$ for an ion at rest. The measured frequency interval $(\nu_2 - \nu_1)_m$ depends on the ion velocity as given below.

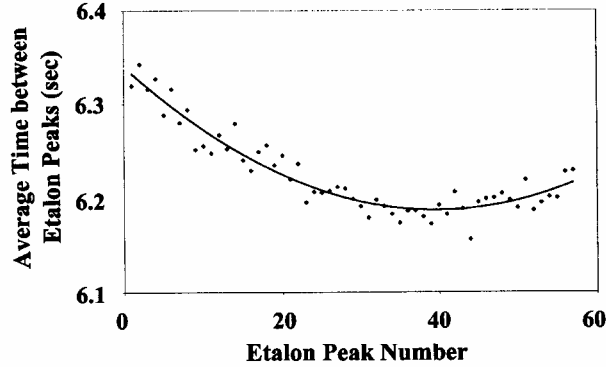$$(\nu_2 - \nu_1)_o = (\nu_2 - \nu_1)_m + \nu_{Corr} \tag{21}$$

Figure 15. Nonlinearity of the Laser Frequency Scan.

The first order correction is $\nu_{Corr} = \pm\beta(\nu_2 - \nu_1)_m$ where the +/- signs apply for counter-/co-propagating ion and laser beams. Hence, the actual hyperfine splittings for an ion at rest were determined using the measured interval and adding ν_{Corr}.

This correction requires knowledge of β, which can be determined in two independent ways. First, β can be found by measuring the difference in laser frequencies required to excite the ions with a co-/counter-propagating laser beam $\nu_{co}/\nu_{counter}$. Using Eqn. 21 one obtains

$$\beta = \frac{\nu_{co} - \nu_{counter}}{\nu_{co} + \nu_{counter}} \qquad (22)$$

This was evaluated to equal $(1.35 \pm 0.02) \times 10^{-3}$ from data obtained using a wavemeter which measured $\nu_{co} = 547{,}170 \pm 15$ GHz and $\nu_{counter} = 545{,}698 \pm 15$ GHz when the laser excited the $^7Li^+$ $1s2s$ $^3S_1(F=3) \rightarrow 1s2p$ $^3P_2(F'=3)$ transition. Alternatively, β was computed to be $(1.3335 \pm 0.0001) \times 10^{-3}$ using the ion accelerating voltage. The two values of β are in agreement but the latter is more precise. Therefore, for each laser scan the data were corrected using the value of β computed from the accelerating voltage.

The uncertainty in β has a negligible effect on ν_{Corr}. For example, the largest frequency interval measured in this experiment was 26.3 GHz, for which $\nu_{Corr} = 35.071 \pm 0.003$ MHz where the error arises because of the uncertainty in β. Higher order corrections in Eqn. 21 are of $O(\beta^2) \times (\nu_{L2} - \nu_{L1}) = 0.047$ MHz. These were negligible compared to the error introduced by the laser frequency scan nonlinearity.

The measured hyperfine splittings of the $^{6,7}Li^+$ $1s2s$ $^3S_1$ and $1s2p$ $^3P_{1,2}$ states are given in Tables 1 and 2. The LIBEO data correspond to a total of 92 scans for $^6Li^+$ and 86 scans for $^7Li^+$ accumulated on 20 different days. The effect of the laser scan nonlinearity was incorporated at the end of the analysis by adding 0.21 MHz in quadrature with the statistical uncertainty of the weighted average. The results for the $1s2p$ $^3P_{1-2}$ fine structure interval are given in Table 3. The LIBEO data are the result of 49 laser scans taken on 7 days.

Table 1. $^6Li^+$ hyperfine splittings.

Level	Interval $(F \rightarrow F')$	Interval (MHz)			Technique	Reference
1s2s $^3S_1$	2→1	5,993	±	6	DT	[42]
		5,997	±	4	LIB	[39]
		6,003.600	±	0.050	LM	[37]
		6,003.66	±	0.51	LIBEO	[30]
		6,003.614	±	0.024	HV	[16]
	1→0	2,998	±	6	DT	[42]
		2,998	±	4	LIB	[39]
		3,001.780	±	0.050	LM	[37]
		3,001.83	±	0.47	LIBEO	[30]
		3,001.765	±	0.038	HV	[16]
1s2p $^3P_1$	2→1	2,889	±	8	QB	[48]
		2,878	±	6	DT	[42]
		2,886	±	4	LIB	[39]
		2,888.98	±	0.63	LIBEO	[30]
		2,888.327	±	0.029	HV	[16]
	1→0	1,318	±	17	QB	[48]
		1,310	±	6	DT	[42]
		1,316	±	8	LIB	[39]
		1,316.06	±	0.59	LIBEO	[30]
		1,317.649	±	0.046	HV	[16]
1s2p $^3P_2$	3→2	4,128	±	9	QB	[48]
		4,113	±	18	DT	[42]
		4,125	±	14	LIB	[39]
		4,127.16	±	0.76	LIBEO	[30]
		4,127.882	±	0.043	HV	[16]
	2→1	2,856	±	8	QB	[48]
		2,861	±	6	LIB	[39]
		2,857.00	±	0.72	LIBEO	[30]
		2,858.002	±	0.060	HV	[16]

3.3 Discussion of results

Tables 1 to 3 compare the LIBEO results with those obtained by previous experiments. Recent Hylleraas Variational (HV) estimates of the fine and hyperfine splittings are included for comparison [7, 16]. Other theory [45-47] has been omitted since it is more than an order of magnitude less accurate.

The LIBEO results for the hyperfine splittings of the $^{6,7}Li^+$ 1s2s $^3S_1$ state are in very close agreement with the best previous measurements as well as theoretical predictions made using the Hylleraas Variational technique [16]. Microwave techniques [37] are particularly well suited to studying this state due to its long lifetime, and the results therefore have the smallest uncertainties. The close agreement of the LIBEO and microwave measurements confirms the validity of the LIBEO technique.

Table 2. $^7Li^+$ hyperfine splittings.

Level	Interval ($F \rightarrow F'$)	Interval (MHz)			Technique	Reference
1s2s $^3S_1$	5/2 → 3/2	19,798	±	24	DT	[41]
		19,796	±	10	LIB	[39]
		19,817.673	±	0.040	LM	[37]
		19,817.1	±	2.6	LIB	[18]
		19,817.90	±	0.73	LIBEO	[30]
		19,817.680	±	0.025	HV	[16]
	3/2 → 1/2	11,872	±	12	DT	[41]
		11,879	±	9	LIB	[39]
		11,890.018	±	0.040	LM	[37]
		11,891.22	±	0.60	LIBEO	[30]
		11,890.013	±	0.038	HV	[16]
1s2p $^3P_1$	5/2 → 3/2	9,932	±	24	DT	[41]
		9,953	±	9	LIB	[39]
		9,965.2	±	0.6	LM	[37]
		9,966.30	±	0.69	LIBEO	[30]
		9,966.14	±	0.13	HV	[16]
	3/2 → 1/2	4,224	±	18	DT	[41]
		4,246	±	20	LIB	[39]
		4,237.8	±	1.0	LM	[37]
		4,239.11	±	0.54	LIBEO	[30]
		4,238.86	±	0.20	HV	[16]
1s2p $^3P_2$	7/2 → 5/2	11,761	±	12	DT	[41]
		11,760	±	6	LIB	[39]
		11,775.8	±	0.5	LM	[37]
		11,774.04	±	0.94	LIBEO	[30]
		11,773.05	±	0.18	HV	[16]
	5/2 → 3/2	9,602	±	12	DT	[41]
		9,598	±	12	LIB	[39]
		9,608.7	±	2.0	LM	[37]
		9,608.90	±	0.49	LIBEO	[30]
		9,608.12	±	0.15	HV	[16]
	3/2 → 1/2	6,182	±	18	DT	[41]
		6,204	±	13	LIB	[39]
		6,203.6	±	0.5	LM	[37]
		6,204.52	±	0.80	LIBEO	[30]
		6,203.27	±	0.30	HV	[16]

Table 3. $^7Li^+$ 1s2p $^3P_{1-2}$ Fine Structure Interval. The values listed were obtained using the most recent theoretical hyperfine intervals [16].

Interval (MHz)			Technique	Reference
62,658	±	28	LIB	[40]
62,678	±	14	Wavemeter	[49]
62,682	±	6	AFM	[17]
62,667.4	±	2.0	LIB	[18]
62,678.41	±	0.65	AFM	[16]
62,679.46	±	0.98	LIBEO	[30]
62,679.4	±	0.5	HV	[7]

The $^6Li^+$ 1s2p $^3P_{1,2}$ hyperfine splittings have been investigated by Doppler tuning an ion beam [41, 42] and saturation spectroscopy [39]. There has also been a quantum beats (QB) experiment [48] that was reported in a thesis. The LIBEO experiment yields data having about an order of magnitude smaller uncertainty. The $^7Li^+$ 1s2p $^3P_{1,2}$ hyperfine intervals have also been investigated using the microwave technique [37]. The microwave results agree well with those of the LIBEO experiment. However, the LIBEO results appear to be somewhat closer to theory [16], most notably for the case of the 1s2p $^3P_2$ (7/2 → 5/2) interval. Indeed, all but one of the 13 measured hyperfine intervals obtained using the LIBEO technique lie within 2σ of the theoretical values. The exception is the measurement of the $^6Li^+$ 1s2p $^3P_2 (1 \to 2)$ interval, which lies 2.7σ from the theoretical result.

Previous experiments have studied transitions to various hyperfine levels of the $^7Li^+$ 1s2p $^3P_{1,2}$ manifolds, which are necessary to determine the 1s2p ^3P fine structure. The values listed in Table 3 were extracted from the experimental data using the most recent theoretically computed hyperfine intervals [16]. The result given in Ref. [49] was obtained using a wavemeter. The experiments quoting the lowest uncertainties use the laser heterodyne technique [18] or measure absolute transition frequencies to various levels [16]. The LIBEO result agrees with the value found by reference [16] and strongly disagrees with the result of the laser heterodyne experiment [18] whose quoted uncertainty is 3σ. It also is closer to the theoretical value than the other experimental results.

4. Spectroscopy of Li D lines

The hyperfine energies E_F corresponding to the various hyperfine levels F contributing to the structure of the lithium D lines are shown in Fig. 16. The positions of
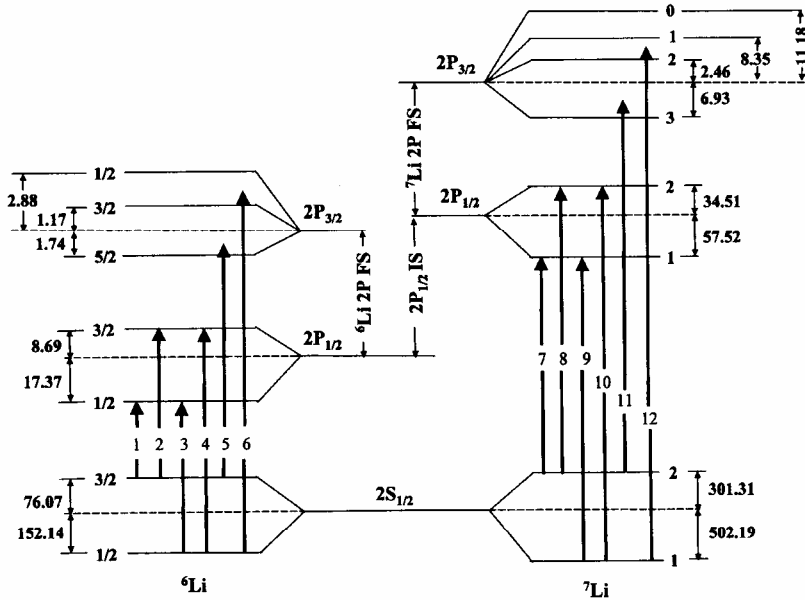
Figure 16. Relevant Energy Levels Affecting Li D Lines. The vertical energy axis is not drawn to scale. The position of the various hyperfine levels is indicated relative to the center of gravity.

the various hyperfine levels are indicated relative to the center of gravity for each state defined by

$$E_{cg} = \sum_F (2F + 1)E_F / \sum_F (2F + 1)$$ (23)

The hyperfine splittings were determined using data found in the literature[50].

4.1 Review of previous work

4.1.1 Level crossing

The level crossing technique (LC), illustrated in Fig. 17 was used by Brog et al [51] to measure the ^{6,7}Li 2P fine structure splitting and by Nagourney et al [52] to measure the magnetic dipole hyperfine constant a of the ^{6}Li $2P_{1/2}$ state listed in Table 4. These experiments are typically done using atoms contained in a vapor cell, heatpipe or atomic beam that is placed in a variable magnetic field. A linear polarizer (LP) polarized light generated by a lamp along the $\hat{x}$ axis. This light excited the $2P_{1/2}$ or $2P_{3/2}$ state. The coils used to generate the magnetic field in the $\hat{z}$ direction are not shown in Fig. 17. A photomultiplier (PMT) monitored the circular polarized (CP) fluorescence emitted from the cell. The splitting between the Zeeman sublevels became larger as the magnetic field was increased. At certain values of the magnetic field, the levels were shifted to the same energy and are said to cross. This crossing changes the amount of circularly polarized fluorescence radiated by the atoms. Brog et al [51] determined the 2P fine structure for ^{6,7}Li with uncertainties of 2 parts in 10^5 while Nagourney et al [52] measured determined the ^{6}Li $2P_{1/2}$ magnetic dipole hyperfine constant with an accuracy of 0.17%. In both cases the uncertainty is due to the inhomogeneity in the magnetic field and its absolute measurement.
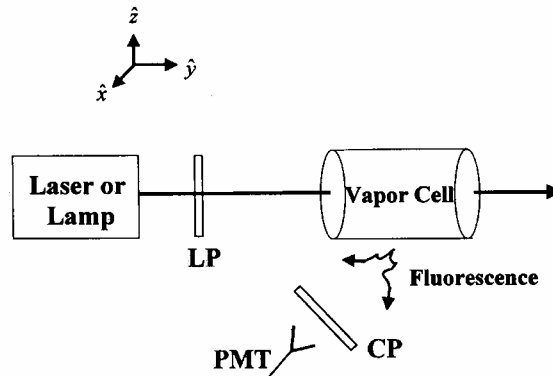
Figure 17. Apparatus for Level Crossing/Optical Double Resonance Experiments

4.1.2 Optical double resonance

Optical double resonance (ODR) uses apparatus similar to that illustrated in Fig. 17. It was used by Ritter et al to measure the magnetic dipole hyperfine constants of the

Table 4. Comparison of Results to Published Data.

Quantity	Interval (MHz)			Technique	Reference
^{6}Li $2S_{1/2}$HFS	228.205259			ABMR	[57]
	228.164	±	0.064	LABEO	[31]
^{6}Li $a(2P_{1/2})$	17.48	±	0.15	ODR	[53]
	17.375	±	0.018	ODR	[50]
	17.8	±	0.3	LC	[52]
	16.8	±	0.7	LAB	[21]
	17.386	±	0.031	LABEO	[31]
^{6}Li 2P FS	10052.76	±	0.22	LC	[51]
	10050.2	±	1.5	LAB	[21]
	10051.62	±	0.20	LAB	[25]
	10053.044	±	0.091	LABEO	[31]
	10050.846	±	0.012	HV	[8]
^{7}Li $2S_{1/2}$HFS	803.5040866			ABMR	[57]
	803.534	±	0.077	LABEO	[31]
^{7}Li $a(2P_{1/2})$	46.17	±	0.35	ODR	[53]
	45.914	±	0.025	ODR	[54]
	46.05	±	0.30	LAB	[21]
	46.010	±	0.025	LABEO	[31]
	45.793			FCPC	[9]
	45.984	±	0.007	MCHF	[10]
	45.945			MCHF	[12]
^{7}Li 2P FS	10053.24	±	0.22	LC	[51]
	10053.184	±	0.058	ODR	[54]
	10056.6	±	1.5	LAB	[21]
	10053.2	±	1.4	LAB	[24]
	10053.40	±	0.20	LAB	[25]
	10052.37	±	0.11	LABEO	[31]
	10051.214	±	0.012	HV	[58]
D1 Isotope Shift	10532	±	5	LAB	[59]
	10534.3	±	0.3	LAB	[21]
	10532.9	±	0.6	FM	[55]
	10526	±	15	FTS	[60]
	10533.13	±	0.15	LAB	[25]
	10534.26	±	0.13	LABEO	[31]
	10528.7			MCHF	[12]
	10534.31	±	0.68	HV	[11]
	10534.12	±	0.07	HV	[58]

^{6,7}Li $2P_{1/2}$ state [53] given in Table 4. In addition, Orth et al [54] used this technique to determine $a(2P_{1/2})$ of ^{6,7}Li as well as the ^{7}Li 2P fine structure splitting. Atoms were placed in a constant uniform magnetic field and excited by a lamp to populate the $2P_{1/2}$ state. A radio frequency signal was then applied to excite transitions among the excited state hyperfine levels when the magnetic field shifted those levels into resonance. These transitions change the amount of circularly polarized fluorescence produced when the $2P_{1/2}$ state radiatively decayed to the $2S_{1/2}$ ground state. Ritter et al [53] measured $a(2P_{1/2})$ for both ^{6,7}Li accurate to 0.8% while Orth's measurements have about an order of magnitude smaller uncertainty. In addition, Orth et al determined the ^{7}Li 2P fine structure splitting to 6 parts in 10^5. The improved accuracy in the experiment by the Orth group was due to their use of a rubidium magnetometer to precisely monitor the magnetic field.

4.1.3 Frequency modulation

Frequency modulation spectroscopy (FM) is illustrated in Fig. 18. Sansonetti et al used this technique to measure the [6,7]Li D1 and D2 isotope shifts [55] listed in Table 4. A ring dye laser beam intersected a lithium atomic beam. Part of the laser beam was diverted to a wavemeter to measure the absolute laser frequency and another part to a Fabry Perot etalon to monitor the laser frequency scan. The rest of the laser beam was split into pump and probe beams that counter-propagated through the lithium beam. The pump beam passed through an acousto-optic modulator (AOM) to avoid feedback of the reflected laser beam that could cause frequency instability. The probe beam passed through an electro-optic modulator (EOM) creating sidebands containing 10% of the laser power and shifted at 20 MHz intervals from the unshifted laser frequency. As the dye laser was scanned across a lithium resonance, the sidebands probed the saturated absorption dip induced by the pump beam. A beat frequency was produced when one of the probe laser sidebands was attenuated due to its absorption by the lithium resonance. The probe laser beam was focused onto a fast photodiode (Fast PD) and the resulting beat signal was measured. The [6,7]Li D1 isotope shift was determined with a statistical uncertainty of 0.6 MHz. The value listed in Table 4 was found using the 2P fine structure measurements of the Orth and Brog groups.
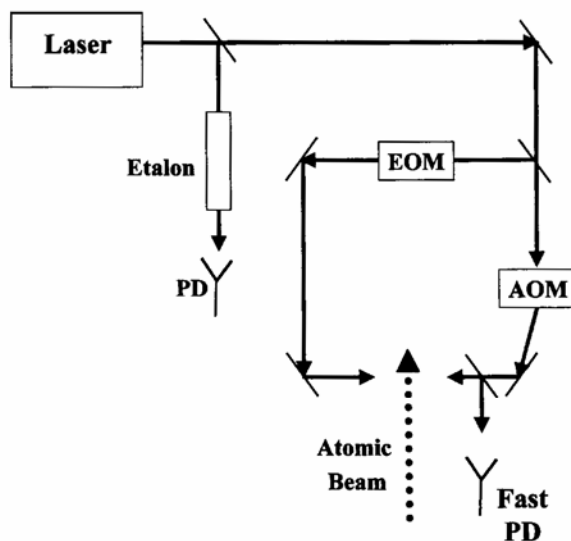

Figure 18. Frequency Modulation Apparatus.

4.1.4 Laser atomic beam spectroscopy

The laser atomic beam method (LAB) uses apparatus similar to that shown in Fig. 19 and is a popular method for measuring frequency intervals. Windholz et al used this technique to determine the $2P_{1/2}$ magnetic dipole hyperfine constant and the 2P fine structure splitting for both [6,7]Li as well as the D1 isotope shift [21-25].

An oven was heated to generate an atomic beam that was collimated by a series of slits. Linearly polarized light from a ring dye laser intersected the atomic beam
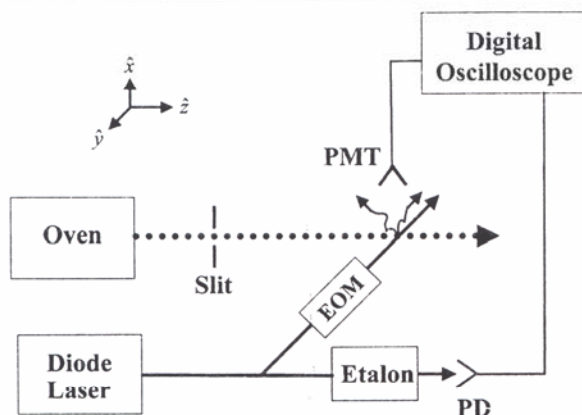
Figure 19. Laser Atomic Beam Spectroscopy Apparatus.

orthogonally to minimize Doppler broadening. Part of the laser beam was incident on a high finesse marker etalon whose free spectral range was determined by a second experiment [23]. The laser was scanned across the lithium resonance. The fluorescence was recorded by a photomultiplier and processed by a lock-in amplifier. The reference signal was provided by a chopper that modulated the dye laser beam. Unfortunately, the determination of the free spectral range of the etalon has been a source of error [21-24] requiring remeasurement [25].

The Windholz group determined the 2P fine structure splitting to be 10050.2 ± 1.5 MHz for ^{6}Li and 10056.5 ± 1.5 MHz for ^{7}Li while a value of 10534.3 ± 0.3 MHz was found for the D1 isotope shift [21]. A later measurement by the same group found a value of 10053.15 ± 0.14 MHz for the ^{7}Li 2P fine structure [22]. In 1995, Sansonetti et al [55] pointed out a possible error in the determination of the free spectral range of the etalon. Subsequent publication by the Windholz group reported 2P fine structure results of 10051.62 ± 0.20 MHz for ^{6}Li, 10053.40 ± 0.20 MHz for ^{7}Li, and a value of 10533.13 ± 0.15 MHz for the ^{6,7}Li D1 isotope shift.

4.2 Laser excitation of atomic beam using an electro-optic modulator

The technique whereby a neutral atomic beam is excited by an electro-optically modulated laser beam (LABEO) is illustrated in Fig. 19. An atomic beam having a divergence of less than 0.5 milliradians was generated by heating a sample of lithium metal to several hundred degrees centigrade. The oven was enclosed in a vacuum chamber pumped using a diffusion pump and a liquid nitrogen trap to a pressure of about 1×10^{-7} torr. The lithium atoms were excited using a diode laser (Tuioptics DL100/670) that produced a laser beam having a power of 12 mW at 670 nm. The laser beam was frequency modulated using either a 6.8 or 9.2 GHz electro-optic modulator as discussed in Section 3.2. The laser beam was linearly polarized along the $\hat{z}$ direction parallel to the atomic beam.

The laser frequency could be scanned up to 15 GHz by adjusting a grating. The linearity of the laser scan was monitored by passing part of the laser beam through a

confocal etalon having a free spectral range of nearly 300 MHz. The etalon was constructed using an invar rod to minimize temperature variation effects. A photodiode (PD) monitored the laser beam transmitted through the etalon.

Fluorescence emitted in the $\hat{x}$ direction was detected by a photomultiplier (PMT - Hamamatsu R928). The photomultiplier and photodiode signals were stored in a digital oscilloscope (Tektronix TDS3052). A single laser scan generated a data file having 10,000 points. A total of 218 separate laser scans were taken using a sample of pure ^{6}Li yielding spectra as shown in Fig. 20. An additional 244 scans as shown in Fig. 21 were taken using a natural sample of lithium. A neutral density filter was inserted in the laser beam during the frequency scan to avoid saturation of the photomultiplier by the D2 fluorescence peak. This also reduced the amount of detected laser scatter as is shown by the change in baseline midway during the scans shown in Figs. 20 and 21. Scans like that shown in Fig. 21 used the 6.8 GHz modulator instead of the 9.2 GHz modulator to avoid overlap of the fluorescence peaks.
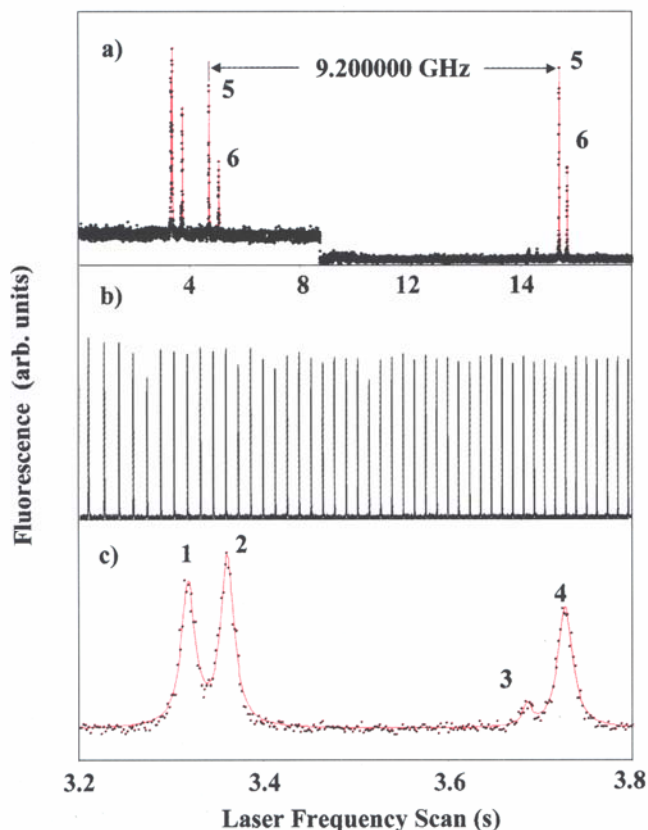
Figure 20. Sample ^{6}Li Laser Scan. a) shows the fluorescence (black dots) taken during a laser frequency scan along with the fitted spectrum (red line). Each transition is excited twice due to electro-optically modulating the laser frequency at 9.200000 GHz. Fig b) shows the transmission of part of the laser beam through an etalon. The first two peaks in a) are actually 4 peaks as shown in c).
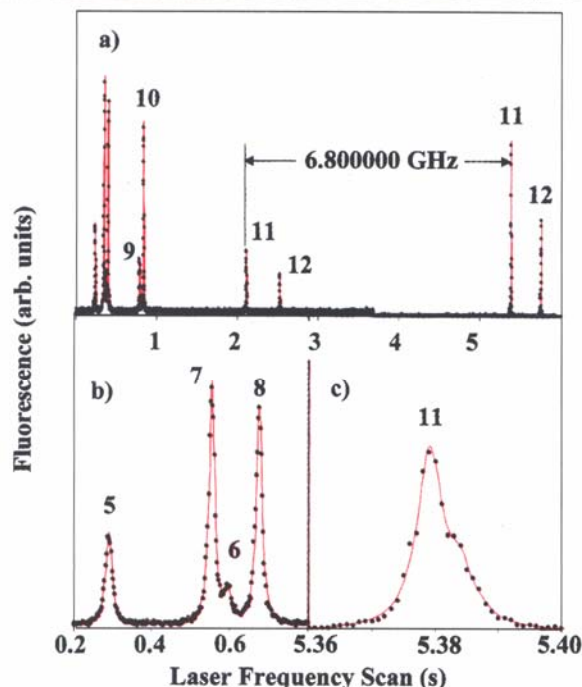
Figure 21. Sample ^{7}Li Laser Scan. a) shows the fluorescence (black dots) taken during a laser scan using a 6.800000 GHz electro-optic modulator along with the fitted spectrum (red line). The first peaks shown in a) are highlighted in b) where peaks 5 and 6 are due to ^{6}Li. c) shows the D2 peak resulting from the excitation of the ^{7}Li $2S_{1/2}$ (F=2) hyperfine level to the $2P_{3/2}$ state.

Data was analyzed using the SOLVER feature of Microsoft Excel (version 9.0). The fluorescence peak positions were found by fitting a sum of Lorentzian functions to the peaks in the spectrum. Similarly, the location of the Fabry Perot transmission peaks were found. The position of a fluorescence peak relative to the nearest Fabry Perot peak was determined using a 5th order polynomial to interpolate between the 6 nearest Fabry Perot peak centers. This was done to account for the nonlinearity of the laser frequency scan. The free spectral range of the etalon was determined using the electro-optic modulation frequency intervals as shown in Figs. 20 and 21.

A stringent test of the experimental technique was to compare the ^{6,7}Li ground state hyperfine splittings with those obtained using an atomic beam magnetic resonance (ABMR) experiment [57]. The ^{6}Li $2S_{1/2}$ hyperfine interval was found by measuring the frequency separating peaks 2 and 4 while the Li $2P_{1/2}$ hyperfine interval was determined using peaks 1 and 2. Peak 3 was not used as it is substantially smaller. For ^{7}Li, the ground state hyperfine splitting found using the separation between peaks 7 and 9 (803.49 ± 0.11 MHz) agreed with that obtained using peaks 8 and 10 (803.57 ± 0.10 MHz). Similarly, the ^{7}Li $2P_{1/2}$ hyperfine interval found from the separation of peaks 7 and 8 (91.94 ± 0.08 MHz) agreed with that found using peaks 9 and 10 (92.10 ± 0.07 MHz).

A complication in determining the ^{6}Li 2P fine structure splitting was that the hyperfine splitting of the ^{6}Li 2P$_{3/2}$ state [53, 54] is smaller than the 5.8 MHz FWHM natural linewidth of the 2P - 2S$_{1/2}$ transition [56]. In addition, the laser does not excite the hyperfine levels equally. For ^{6}Li, the 2S$_{1/2}$ (F=1/2) hyperfine level can only be laser excited to the 2P$_{3/2}$ (F=1/2, 3/2) hyperfine levels. Moreover, these two hyperfine levels contribute differently to the observed fluorescence due to their respective transition Clebsch Gordan coefficients. A computer program was written to model this optical pumping effect resulting from repeated laser excitation and fluorescence decay as an atom passed through the laser beam [28]. It was found that the fluorescence signal observed by exciting the 2S$_{1/2}$ (F=1/2) level to the 2P$_{3/2}$ state is +1.90 MHz above the 2P$_{3/2}$ center of gravity indicated in Fig. 16. Similarly, the fluorescence signal observed by exciting the 2S$_{1/2}$ (F=3/2) level to the 2P$_{3/2}$ state is 1.27 MHz below the 2P$_{3/2}$ center of gravity. The results listed in Table 4 for the ^{6}Li 2P fine structure have been corrected for this effect. A test of these corrections was made by determining the 2S$_{1/2}$ hyperfine splitting using the D2 line. The measured value for the separation between peaks 5 and 6 in Fig. 20 was 231.327 ± 0.050 MHz. Taking into account the two corrections given above yields a ground state hyperfine splitting of 228.157 ± 0.050 MHz, in excellent agreement with the accepted value.

For the ^{7}Li D2 line, the laser excitation partially resolves the 2P$_{3/2}$ (F = 1, 2, 3) hyperfine splittings although the F = 3 hyperfine level dominates the fluorescence signal as shown in Fig. 21c. Peak 11 was fitted using three Lorentzians where the relative center frequencies were constrained to equal the intervals separating the F = 1 & 2 and F = 2 & 3 hyperfine levels of the 2P$_{3/2}$ state [50]. The ^{7}Li 2P fine structure was determined by measuring the separation of peaks 10 and 11. Peak 12 was not analyzed because the intervals separating the 2P$_{3/2}$ (F = 0, 1, 2) levels are smaller than is the case for peak 11 making it more difficult to model precisely. The D1 isotope shift was determined by measuring the separation of peaks 5 and 7 shown in Fig. 21 and using the ^{6}Li 2P fine structure splitting as determined in Fig. 20.

4.3 Discussion of results

Table 4 shows excellent agreement of the LABEO results with the published data. The listed uncertainties are one standard deviation of the data from the average value. The results for the ^{6,7}Li 2P$_{1/2}$ magnetic dipole hyperfine constants have an uncertainty comparable to the best published values. The value for ^{7}Li a(2P$_{1/2}$) is 96 kHz higher than that obtained in an optical double resonance experiment [50] where the uncertainty of each measurement is 25 kHz. It is interesting that recent predictions found using Multiconfiguration Hartree Fock (MCHF) theory [10, 12] lie between the two most precise experimental results while a result computed using the Full Core plus Correlation (FCPC) technique [9] is somewhat lower than the measured values.

The LABEO result for the ^{6}Li 2P fine structure splitting has the smallest uncertainty of any experimental determination. It agrees with the result of a level crossing experiment unlike the values found by laser atomic beam experiments. The LABEO result for the ^{7}Li 2P fine structure splitting is slightly smaller than that found previously. This may be due to the partial resolution of the 2P$_{3/2}$ hyperfine splitting described in section 4.2 as it is not clear how some of the other experiments accounted for this effect. Table 4 also lists the estimates obtained using the Hylleraas Variational theory for the

^{6,7}Li 2P fine structure splittings [8]. The listed uncertainty for these results represents the computation error. These results are 1-2 MHz below the experimental data which is not surprising as only terms in the Hamiltonian up to $O(\alpha^3)$ times the Rydberg energy were considered. For the case of helium, comparable terms of $O(\alpha^4)$ contribute several MHz to the fine structure splitting [6, 7].

The LABEO result for the D1 isotope shift is over 1 MHz higher than the most accurate laser atomic beam result as well as the value found using the frequency modulation technique. A recent experiment using Fourier transform spectroscopy (FTS) agrees with the other measurements but has a much larger uncertainty. However, the LABEO value agrees very well with the result of the latest Hylleraas Variational calculation [58] which refines an earlier estimate that took into account the finite nuclear size as well as QED terms up to order $(\mu/M)\alpha^3$ [11]. All of the experimental values are significantly higher than a result found using multiconfiguration Hartree Fock theory [12].

5. Conclusions

The results for the fine and hyperfine intervals of the Li$^+$ 1s2p ^{3}P state obtained using the LIBEO technique are in excellent agreement with the latest Hylleraas Variational theory. The discrepancy for the ^{7}Li$^+$ 1s2p ^{3}P$_{1,2}$ fine structure interval as measured by two experimental groups has been definitively resolved. This strongly suggests that the LIB experiment done by the group by Rong et al has a systematic effect that is not understood. An advantage of the LIBEO method is that it does not measure absolute transition frequencies like the AFM technique and therefore does not require access to a national standards laboratory having multiple lasers whose frequencies are ultrastable.

In the case of the Li D lines, the LABEO experiment determined the ^{6,7}Li isotope shift, fine structure and hyperfine splittings of the 2S$_{1/2}$ and 2P$_{1/2}$ states. The results are consistent with very accurate measurements of the ground state hyperfine splitting. The value obtained for the D1 isotope shift disagrees with previous laser atomic beam measurements but is very close to the latest theoretical calculation. However, the theoretical results for the ^{6,7}Li 2P fine structure values are significantly below all of the experimental results. This strongly indicates that theory must be refined to take into account higher order contributions to the Hamiltonian.

A key advantage of the LIBEO/LABEO technique is that it does not require calibration of an etalon's free spectral range by a secondary experiment that has been shown to be problematic. Each scan is separately calibrated using the electro-optic modulation frequency. Hence, LIBEO/LABEO is insensitive to temperature or pressure fluctuations, vibrations etc. that can perturb the etalon calibration. An etalon is only used to minimize effects due to scanning nonlinearity of the laser frequency. The use of a frequency modulated laser beam also permits more accurate determination of large frequency intervals since one measures a smaller interval separating a peak generated by a laser frequency sideband. For example, a 9.2 GHz electro-optic modulator permits the determination of a 10 GHz fine structure splitting by measuring a smaller 0.8 GHz interval. This significantly reduces possible systematic effects since the modulation frequency can be conveniently generated with high accuracy. Hence, the LIBEO/LABEO experimental method has wide applicability for precision laser spectroscopic measurements.

6. Acknowledgements

References

1.   H. Bethe & E. Salpeter, *Quantum Mechanics of One and Two Electron Atoms,* (Plenum, New York, 1957).
2.   W. Frieze, E. Hinds & V. Hughes, Phys. Lett. **78A**, 322 (1980).
3.   G. Drake, Adv. At. Mol. Opt. Phys. **18**, 399 (1982).
4.   P. Cancio et al, *Atomic Physics 16*, edited by W. Baylis & G. Drake (AIP, New York, 1999).
5.   M. George, L. Lombardi & E. Hessels, Phys. Rev. Lett. **87**, 173002 (2001).
6.   G. Drake, *Atomic, Molecular & Optical Physics Handbook*, edited by G. Drake (AIP, New York, 1996).
7.   T. Zhang, Z. Yan & G. Drake, Phys. Rev. Lett. **77**, 1715 (1996).
8.   Z. Yan & G. Drake, Phys. Rev. Lett. **79** , 1646 (1997).
9.   X. Guan & Z. Wang, Eur. Phys. J. D **2**, 21 (1998).
10. N. Yamanaka, J. Phys. Soc. Japan **68**, 2561 (1999).
11. Z. Yan & G. Drake, Phys. Rev. A **61**, 22504-1 (2000).
12. M. Goedfroid, C. Fischer & P. Jonsson, J. Phys. B **34**, 1079 (2001).
13. H. Berry, E. Pinnington & J. Subtil, Phys. Rev. A **10**, 1065 (1974).
14. R. Holt et al, Phys. Rev. A **22**, 1563 (1980).
15. R. Grieser et al, Appl. Phys. B **59**, 127 (1994).
16. E. Riis et al, Phys. Rev. A **49**, 207 (1994).
17. E. Riis et al, Phys. Rev. A **33**, 3023 (1986).
18. H. Rong et al, Z. Phys. D. **25**, 337 (1993).
19. H. Rong et al, Eur. Phys. J. D **3**, 217 (1998).
20. H. Rong et al, Opt. Comm. **201**, 345 (2002).
21. L. Windholz et al, Z. Phys. D. **16**, 41 (1990).
22. L. Windholz & U. Umfer, Z. Phys. D. **29**, 121 (1994).
23. H. Jager et al, Opt. Eng. **29**, 42 (1990).
24. C. Umfer, L. Windholz & M. Musso, Z. Phys. D **25**, 23 (1992).
25. W. Scherf et al, Z. Phys. D **36**, 31 (1996).
26. W. van Wijngaarden, Adv. At. Mol. & Opt. Phys. **36**, 141 (1996).
27. W. van Wijngaarden, Proc. of Atomic Physics **16**, 305 (1998).
28. J. Walls, Masters Thesis, York University (2001).
29. J. Clarke, Ph.D. Thesis, York University (2002).
30. J. Clarke & W. van Wijngaarden, submitted for publication, (2002).
31. J. Walls et al, submitted for publication, (2002).
32. C. Cohen-Tannoudji, B. Diu & F. Laloë, *Quantum Mechanics*, (Wiley, New York, 1977).
33. A. Wapstra & G. Audi, Nucl. Phys. A **432**, 1 (1985).
34. P. Mohr, *Atomic, Molecular & Optical Physics Handbook*, edited by G. Drake (American Institute of Physics, New York, 1996).
35. J. Sapirstein, *Atomic, Molecular & Optical Physics Handbook*, edited by G. Drake American Institute of Physics, New York, 1996).
36. R. Knight & M. Prior, Phys. Rev. A **21**, 179 (1980).
37. J. Kowalski et al, Hyperfine Interactions **15/16**, 159 (1983).
38. G. Drake, Phys. Rev. A **19**, 1387 (1979).
39. R. Bayer et al, Z. Phys. A. **292**, 329 (1979).
40. R. Bayer, Staatsexamensarbeit, University of Heidelberg (1979).

41. B. Fan, A. Lurio & D. Grischkowsky, Phys. Rev. Lett. **41**, 1460 (1978).
42. B. Fan, D. Grischkowsky & A. Lurio, Opt. Lett. **4**, 233 (1979).
43. S. Gerstenkorn & P. Luc, *Atlas du Spectra d'Absorption de la Molecule de l'Iode (14 800 - 20 000 cm⁻¹)*, (Editions du CNRS, 1978).
44. R. Holt et al, Rev. Sci. Instrum. **52**, 157 (1981).
45. A. Jette, T. Lee & T. Das, Phys. Rev. A **9**, 2337 (1974).
46. W. Johnson, K. Cheng & D. Plante, Phys. Rev. A **55**, 2728 (1997).
47. B. Schiff, Y. Accad & C. Perkeris, Phys. Rev. A **1**, 1837 (1970).
48. W. Wittmann, Doctoral Thesis, Freie Universität Berlin (1977).
49. R. Schwarzwald, Diploma Thesis, University of Heidelberg (1982).
50. E. Arimondo, M. Inguscio & P. Violino, Rev. Mod. Phys. **49**, 31 (1977).
51. K. Brog, T. Eck & H. Wider, Phys. Rev. **153**, 91 (1966).
52. W. Nagourney & W. Happer, Phys. Rev. A **17**, 1394 (1978).
53. G. Ritter, Can. J. Phys. **43**, 770 (1965).
54. H. Orth, H. Ackermann & E. Otten, Z. Phys. A, **273**, 221 (1975).
55. C. Sansonetti et al, Phys. Rev. A **52**, 2682 (1995).
56. J. Carlsson & L. Sturesson, Z. Phys. D **14**, 281-287 (1989).
57. A. Beckmann, K. Bokle & D. Elke, Z. Phys. **270**, 173 (1974).
58. Z. Yan & G. Drake, submitted for publication (2002).
59. R. Mariella, Appl. Phys. Lett. **35**, 580 (1979).
60. L. Radziemski, R. Engleman & J. Brault, Phys. Rev. A **52**, 4462 (1995).